Single-cell transcriptomics of the human retinal pigment epithelium and choroid in health and macular degeneration

Andrew P. Voigt[a,b], Kelly Mulfaul[a,b], Nathaniel K. Mullin[a,b], Miles J. Flamme-Wiese[a,b], Joseph C. Giacalone[a,b], Edwin M. Stone[a,b], Budd A. Tucker[a,b], Todd E. Scheetz[a,b], and Robert F. Mullins[a,b,1]

[a]Department of Ophthalmology and Visual Sciences, The University of Iowa Carver College of Medicine, Iowa City, IA 52242; and [b]Institute for Vision Research, The University of Iowa, Iowa City, IA 52242

Edited by Jeremy Nathans, Johns Hopkins University School of Medicine, Baltimore, MD, and approved October 18, 2019 (received for review August 30, 2019)

The human retinal pigment epithelium (RPE) and choroid are complex tissues that provide crucial support to the retina. Disease affecting either of these supportive tissues can lead to irreversible blindness in the setting of age-related macular degeneration. In this study, single-cell RNA sequencing was performed on macular and peripheral regions of RPE-choroid from 7 human donor eyes in 2 independent experiments. In the first experiment, total RPE/choroid preparations were evaluated and expression profiles specific to RPE and major choroidal cell populations were identified. As choroidal endothelial cells represent a minority of the total RPE/choroidal cell population but are strongly implicated in age-related macular degeneration (AMD) pathogenesis, a second single-cell RNA-sequencing experiment was performed using endothelial cells enriched by magnetic separation. In this second study, we identified gene expression signatures along the choroidal vascular tree, classifying the transcriptome of human choriocapillaris, arterial, and venous endothelial cells. We found that the choriocapillaris highly and specifically expresses the regulator of cell cycle gene (*RGCC*), a gene that responds to complement activation and induces apoptosis in endothelial cells. In addition, *RGCC* was the most upregulated choriocapillaris gene in a donor diagnosed with AMD. These results provide a characterization of the human RPE and choriocapillaris transcriptome, offering potential insight into the mechanisms of choriocapillaris response to complement injury and choroidal vascular disease in age-related macular degeneration.

choroid | choriocapillaris | single cell | age-related macular degeneration

In human vision, the neural retina serves as a specialized light-sensitive tissue necessary for visual perception. Photoreceptor cells located in the outer retina perform phototransduction, the process of converting a photon of light into a neurochemical signal that will eventually be interpreted as vision. The highly precise physiology of photoreceptor cells relies on support from 2 underlying tissues: the retinal pigment epithelium (RPE) and choroid.

The RPE consists of a monolayer of pigmented cells that play an essential role in supporting the retina. The RPE promotes proper photoreceptor cell function by enzymatically preparing retinoids needed for visual transduction (1) and phagocytizing phototransduction machinery (photoreceptor outer segments), allowing for its renewal (2). In addition, the RPE absorbs excess light to minimize nonspecific light scattering (3), quenches oxidative stress (4), and provides metabolic support to photoreceptor cells (5).

The RPE overlays the choroid, a heterogeneous connective tissue that supports both the RPE and the outer retina. The choroid houses several cells types found in other connective tissues, including fibroblasts, melanocytes, contractile pericytes/smooth muscle cells, and infiltrating immune cells (6). In addition, the choroid contains a rich vascular system that has the critical role of providing oxygenated blood to the RPE and photoreceptor cells. This choroidal vascular bed provides ∼85% of blood to the retina (7) and anatomically consists of a very dense superficial capillary system known as the choriocapillaris, as well as underlying medium (Sattler's layer) and large-diameter (Haller's layer) vessels. The choriocapillaris is an exceptionally specialized capillary bed that is imperative for proper retinal function. Developmentally, the choriocapillaris arises from distinct hemangioblast precursor cells, unlike the underlying choroidal vessels (8). In contrast to the retinal vasculature, the choriocapillaris has large-diameter vessels that are fenestrated (6), permitting the dissemination of small molecules through the endothelial layer. Functionally, the choriocapillaris highly expresses HLA class I self-peptides (9), ICAM-1 (10), and carbonic anhydrase 4 (CA4) (11), which help regulate the metabolic and inflammatory environment within the choroid and the tissues it supports.

As the RPE and choroid provide crucial support to the retina, diseases affecting the RPE and choroid are responsible for many of the most common causes of vision loss. In particular, age-related macular degeneration (AMD) is a major cause of irreversible blindness in the western world, with a prevalence of 12.3 to 30% in individuals of European descent (12). Dysfunction of both the RPE and the choroid have been widely implicated in

Significance

The retinal pigment epithelium and the choroid are complex tissues whose dysfunction can lead to irreversible visual loss. In this study, single-cell RNA sequencing of both of these tissues was performed to characterize gene expression patterns specific to the retinal pigment epithelium and all major choroidal cell populations. Unique gene expression signatures of arterial, venous, and choriocapillaris vascular beds within the choroid were identified. *RGCC*, a gene that responds to complement and has been shown to induce endothelial apoptosis, was specifically expressed in choriocapillaris endothelial cells. This study provides potential insight into the molecular mechanisms of choroidal vascular disease and its contribution to age-related macular degeneration.

Author contributions: A.P.V., K.M., N.K.M., M.J.F.-W., J.C.G., E.M.S., B.A.T., T.E.S., and R.F.M. designed research; A.P.V., K.M., N.K.M., M.J.F.-W., J.C.G., and R.F.M. performed research; J.C.G. and B.A.T. contributed new reagents/analytic tools; A.P.V., K.M., N.K.M., E.M.S., B.A.T., T.E.S., and R.F.M. analyzed data; and A.P.V., K.M., N.K.M., M.J.F.-W., J.C.G., E.M.S., B.A.T., T.E.S., and R.F.M. wrote the paper.

The authors declare no competing interest.

This article is a PNAS Direct Submission.

Data deposition: The data reported in this paper have been deposited in the Gene Expression Omnibus (GEO) database, https://www.ncbi.nlm.nih.gov/geo (accession no. GSE135922).

[1]To whom correspondence may be addressed. Email: mullinsrf@gmail.com.

This article contains supporting information online at www.pnas.org/lookup/suppl/doi:10.1073/pnas.1914143116/-/DCSupplemental.

First published November 11, 2019.

AMD pathogenesis. RPE degeneration has been purported to lead to downstream formation of drusen and inflammation (13), and oxidative stress secondary to RPE dysfunction has been postulated as a major source of photoreceptor cell damage (14). Within the choroid, vascular dropout has been observed to precede RPE perturbations (15–17), and such vascular disease has been proposed as the seminal event leading to subsequent retinal degeneration. In particular, the membrane attack complex (MAC), a lytic multiprotein pore forming complex that assembles as a result of complement activation, is elevated in the choriocapillaris with both advancing age and AMD (18).

To date, most gene expression studies of the RPE and the choroid have utilized mRNA from pooled RPE and choroidal cell lysates, as these tissues are technically challenging to separate (19–23). Moreover, the cellular diversity of the choroid prevents defining gene expression patterns unique to individual cell populations, hampering further understanding of normal choroidal physiology. Recent advances in single-cell RNA sequencing are capable of addressing these limitations and provide a powerful approach to study gene expression within complex tissues such as the choroid. In this manuscript, 2 single-cell RNA-sequencing experiments from 7 human donor eyes were performed to study gene expression in the RPE/choroid, with a particular focus on choroidal endothelial cells. Gene expression patterns of the RPE and the major choroidal cell types were identified, and unique expression signatures for endothelial cell populations along the choroidal vascular tree were defined.

Results

Experiment Overview and Single-Cell RNA Sequencing. Three human donors were included in this initial study (Table 1). For each donor, 8-mm punches were obtained from the macula and the periphery. The combined RPE/choroid samples were dissected from the retina and the sclera, and the RPE/choroid underwent gentle dissociation into single-cell suspensions. Single-cell RNA sequencing was performed on each of the 6 dissociated RPE/choroid samples from donors 1 to 3. A total of 4,335 cells were recovered after filtering, of which 2,167 cells originated from the macula and 2,168 cells originated from the periphery. After normalization and cell-to-cell regression to minimize batch effect, graph-based clustering using the first 11 principal components was performed to cluster cells with similar gene expression profiles. Uniform manifold approximation and projection (UMAP) dimensionality reduction was utilized to visualize the 11 identified clusters, ranging in size from 33 cells to 1341 cells (Fig. 1*A*). All clusters were composed of cells from each donor, with the exception of cluster 1, the smallest cluster, which did not contain any cells from donor 2 (*SI Appendix*, Table S1).

The human choroid is a complex vascular tissue that supplies oxygen to the overlying RPE and outer retina (Fig. 1*B*). A list of genes previously reported to be expressed in the RPE and in a variety of choroidal cell types was compiled (*SI Appendix*, Table S2), and the expression of these genes was compared across all clusters (Fig. 1*C*).

Cluster Classification. The cells in clusters 1 and 2 are interpreted as Schwann cells, with high expression of the proteolipid protein gene (*PLP1*), which encodes the most abundant protein in myelin (Fig. 1*C*). Cluster 1, the smallest cluster observed in this experiment, consisted of only 33 cells from 2 donors (*SI Appendix*, Table S1). Cluster 2 was much larger, consisting of 489 cells. Interestingly, 64% of cells in cluster 2 originated from the macular RPE/choroid of donor 3, the donor diagnosed with neovascular AMD.

Cluster 3 is interpreted as being derived from melanocytes, which are responsible for choroidal pigmentation but have a largely unknown function within the choroid (6). Cells in this cluster demonstrate specific expression of the melanocyte-specific trafficking protein *MLANA* (Fig. 1*C*), as well as melanocyte protein (*PMEL*), tyrosinase-associated protein-1 (*TYRP1*), and dopachrome tautomerase (*DCT*) (*SI Appendix*, Fig. S1).

Cluster 4 is proposed to consist of endothelial cells, with high expression of *VWF* (Fig. 1*C*), *CD34*, and *ICAM2* (*SI Appendix*, Fig. S1). Endothelial cells are surrounded by contractile smooth muscle cells (in large vessels) and pericytes (in capillaries). Cells with smooth muscle expression patterns constituted cluster 5, with high expression of smooth muscle α-actin (*ACTA2*) (Fig. 1*C*) and *RGS5* (*SI Appendix*, Fig. S1). Cluster 6 is interpreted as containing fibroblasts, with high expression of *IGF2* (Fig. 1*C*). Cluster 7 consists of cells from the RPE, with abundant *RPE65* and *BEST1* expression (Fig. 1*C*).

Clusters 8 to 11 are interpreted as circulating and resident leukocytes, with high expression of *PTPRC* (which encodes the cell surface gene product CD45, or leukocyte common antigen, expressed on all classes of leukocytes) (Fig. 1*C*). Lymphocytes segregated into clusters 8 and 9, with *CD79A*-expressing B cells forming cluster 8 while *CD2*-expressing T cells/NK cells formed cluster 9. Cluster 10 consists of monocytes and/or macrophages, with high expression of the activated macrophage inflammatory cytokine *AIF1*. Cluster 11 is interpreted as *KIT*-expressing mast cells.

For each population, the expression of several additional cell-specific genes was investigated and largely corroborates our cluster classifications (*SI Appendix*, Fig. S1). To provide a central reference for cell-specific expression patterns, differential expression was performed to identify cell type-specific genes in each cluster and merged with cluster-specific expression data (Dataset S1).

Differential Expression between Clusters. As Schwann cells segregated into 2 clusters, differential expression analysis between clusters 1 and 2 was performed to identify genes specific for potential Schwann cell subclasses (*SI Appendix*, Fig. S2 and Dataset S2).

Table 1. Information for each of the 7 donors included in the single-cell RNA-sequencing studies

Donor	Age	Sex	Eye	Cause of death	Time to preservation	Ophthalmic notes	Experiment
Donor 1	54	M	OD	Cardiac arrest	5:29	Mild cataracts, normal macula	1) Unselected RPE/choroid
Donor 2	82	F	OD	Cardiopulmonary arrest	4:18	Thick basal laminar deposits in contralateral eye, no advanced disease	1) Unselected RPE/choroid
Donor 3	79	M	OS	Sepsis	7:28	Neovascular AMD	1) Unselected RPE/choroid
Donor 4	92	F	OD	Respiratory distress	5:04	Neovascular AMD	2) $CD31^+$ selection
Donor 5	80	M	OS	Cardiac arrest secondary to respiratory failure	5:50	Normal macula contralateral eye	2) $CD31^+$ selection
Donor 6	75	F	OS	COPD	6:44	Minor focal basal deposits contralateral eye	2) $CD31^+$ selection
Donor 7	77	M	OD	Lung cancer	4:48	Normal macula contralateral eye	2) $CD31^+$ selection

When possible, histological analysis was completed on the contralateral macula to supplement clinical ophthalmologic history. OD, oculus dexter (right eye); OS, oculus sinister (left eye).

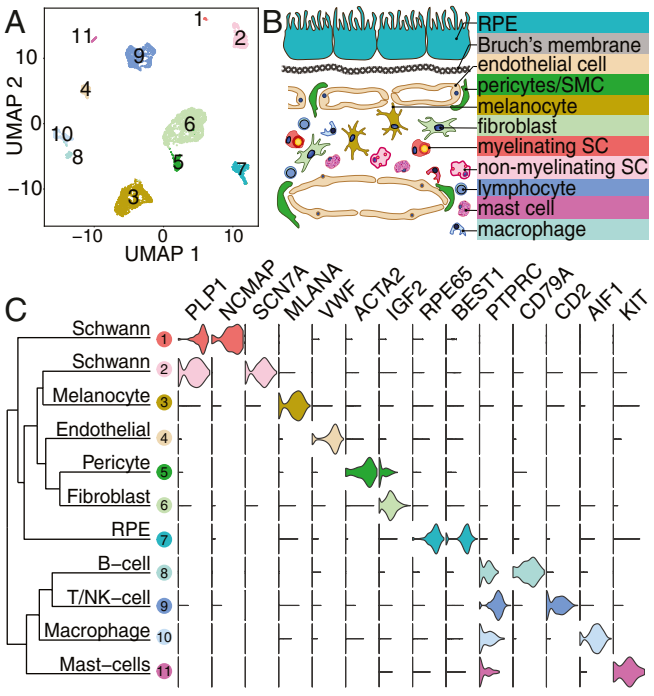

Fig. 1. Identification of RPE and choroidal cell populations. (*A*) UMAP dimensionality reduction was performed to visualize the 11 identified RPE and choroidal clusters. A total of 4,335 cells were recovered after filtering. (*B*) An overview schematic of the cell populations found within the choroid. SC, Schwann cell; SMC, smooth muscle cell. (*C*) For each cluster, the average RNA expression of each gene was calculated. The top 100 most enriched transcripts in each cluster were identified and compiled, and the average expression of these transcripts was used as input for hierarchical clustering analysis. Violin plots of genes previously reported to be enriched in RPE and choroidal cell populations are plotted alongside the dendrogram.

Both Schwann cell clusters express the canonical Schwann cell genes *PLP1* and transcription factor *SOX10*. The 2 most up-regulated genes in Schwann cell cluster 1 were myelin protein zero (*MPZ*) and myelin basic protein (*MBP*), both of which encode proteins found in myelinating Schwann cells. In contrast, nonmyelinating Schwann cells express *SCN7A*, *NGFR*, *NCAM1*, and *L1CAM*, all of which were enriched in cluster 2. The majority (64%) of cells in cluster 2 originated from the macula of the donor with neovascular AMD (donor 3). In order to investigate whether the nonmyelinating Schwann cell gene expression signature was driven predominantly from this patient with AMD, the expression of nonmyelinating genes was compared across all 6 libraries. The nonmyelinating Schwann cell genes were expressed at similar levels across all samples, suggesting that nonmyelinating Schwann cells were present in all donors (*SI Appendix*, Fig. S2*F*).

As 64% of the nonmyelinating Schwann cells originated from the macula of the donor with neovascular AMD (donor 3), we next performed differential expression analysis to determine whether these cells harbored unique patterns of gene expression. Nonmyelinating Schwann cells from the macula of donor 3 were compared to macular nonmyelinating Schwann cells from the remaining 2 donors (*SI Appendix*, Fig. S2*G* and Dataset S3). Interestingly, the most up-regulated gene in the AMD-donor Schwann cells was *CFD* (logFC = 2.35). *CFD* encodes the complement factor D protein, an activator of the alternative complement pathway, which has been previously implicated in AMD pathogenesis (24). As only 1 AMD donor was included in this initial study, such differential expression results are valuable for hypothesis generation, but further experiments will be necessary to determine the extent to which these changes apply to the entire AMD population.

Differential Expression between Macula and Periphery. Within each cell population, differential expression analysis was additionally completed between cells originating from the macular versus the peripheral punches (Dataset S4). Regional gene expression differences between RPE cells and pericytes are highlighted (Fig. 2). *PDK4*, a metabolic enzyme associated with pericyte proliferation and diminished endothelial–pericyte interaction (25), was significantly enriched in macular derived pericytes. In contrast *APOE*, a metabolic protein that has been reported to decrease pericyte mobility, was enriched in peripheral pericytes (26) (Fig. 2*A*). Macular-derived RPE cells had enriched expression of *CXCL14*, a chemokine that regulates immune cell migration (27) and increases angiogenesis (28). Additionally, *WFDC1*, which encodes a protease inhibitor previously shown to be increased in macular RPE (29), demonstrated increased expression within the macula. Peripheral RPE cells were notable for increased expression of *TFPI2*, which promotes RPE proliferation in vitro (30), and *IGFBP5*, which has been associated with reduced neovascularization (31) (Fig. 2*B*).

The genes identified to be differentially expressed in pericytes and RPE were compared to our previous investigation of bulk gene expression between macular and peripheral RPE/choroid samples (Fig. 2). With the exception of *CCL19* expression in pericytes, bulk RNA sequencing recapitulates the regional enrichment of these genes observed at the single-cell level.

Choroidal versus Retinal Endothelial Genes. Recently, we performed single-cell RNA sequencing on retinas from 3 human donors (32). Two of the donors in the initial retina study (donors 2 and 3)

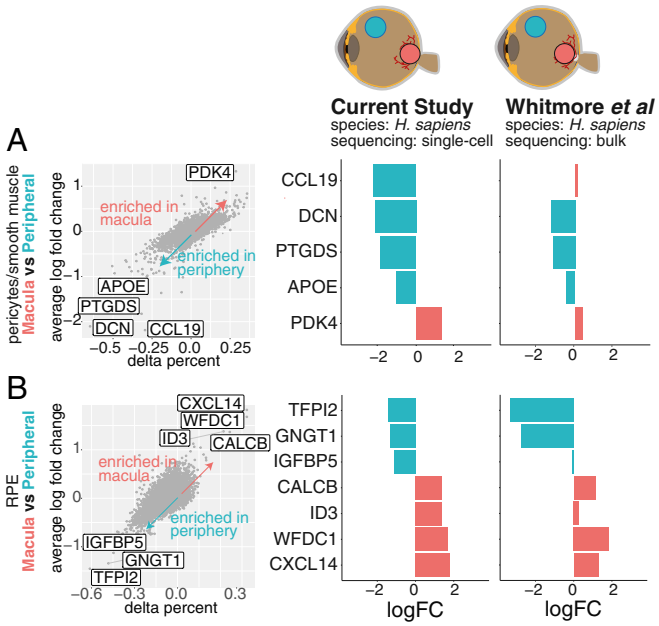

Fig. 2. Differential expression of macular versus peripheral pericytes and RPE cells. Differential expression was performed between smooth muscle cells/pericytes (*A*) and RPE cells (*B*) of macular and peripheral origin. For each gene, the average log fold change and the percentage of cells that express the gene above background are compared between the 2 clusters (*Right*). For example, a delta percent of +0.25 indicates that 25% more cells of macular pericytes express the gene above background than peripheral pericytes. Expression patterns from the most enriched genes were compared to bulk RNA expression from pooled RPE/choroid cell lysates (19), which largely corroborates the regional expression differences observed in cell populations identified by single-cell RNA sequencing.

were included in the current investigation of RPE/choroid gene expression (donors 1 and 2, respectively). As both the retina and the choroid have isolated populations of endothelial cells, we aggregated the retina and RPE/choroid datasets from these donors to compare endothelial gene expression between these 2 tissues. A total of 413 endothelial cells were recovered after filtering, with 254 cells originating from the retina and 159 cells originating from the choroid. Two clusters of endothelial cells were identified that were largely distinct based on tissue of origin (Fig. 3 *A* and *B*). Differential expression analysis was performed between endothelial cells originating from the retina versus the choroid (Fig. 3 *C* and *D* and Dataset S5). Retinal endothelial cells were enriched in expression of regulators of barrier permeability, such as *CLDN5*, which regulates endothelial cell permeability, and *SLC2A1*, which encodes the major glucose transporter in the blood–brain barrier (33). In contrast, choroidal endothelial cells were enriched in several genes involved in leukocyte recruitment and adhesion, including *VCAM1*, *CCL2*, *SELP*, and *ICAM1*. Choroidal endothelial cells also demonstrated higher expression of *CLU*, a negative regulator of complement activation (34).

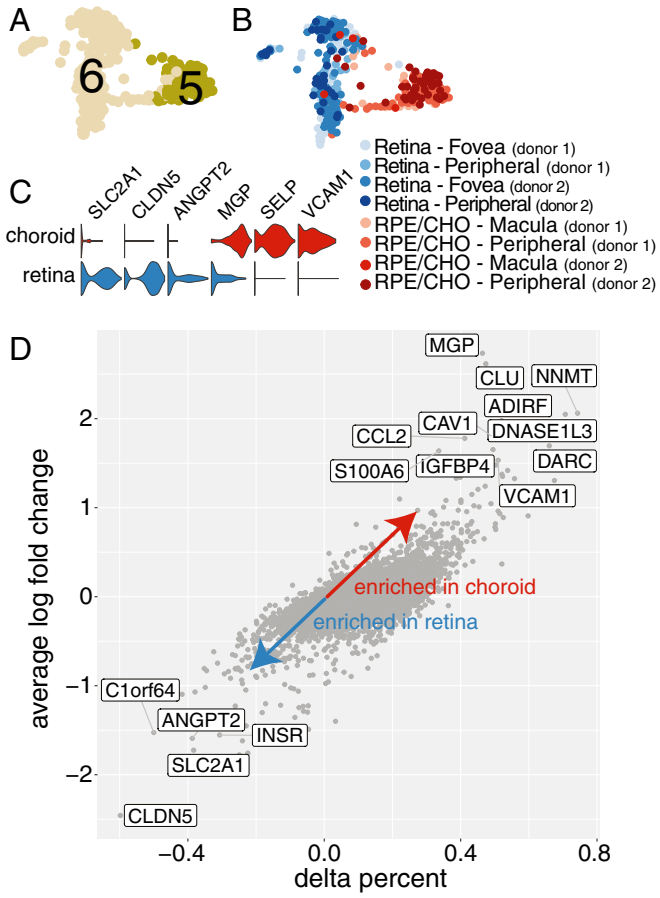

Fig. 3. Retinal versus choroidal endothelial cell gene expression. (*A*) Two of the donors in this investigation (donors 1 and 2) were included in a single-cell RNA-sequencing study of human retina (donors 2 and 3 of that report). The RPE/choroid and retinal data were aggregated for these donors. Two clusters of endothelial cells (clusters 5 and 6) consisting of 413 total cells were identified. (*B*) The clusters were largely distinct based on tissue of origin, with retinal endothelial cells colored in blue and choroidal endothelial cells colored in red. (*C* and *D*) Differential expression between retinal and choroidal endothelial cells was performed. For each gene, the average log fold change and the percentage of cells that express the gene above background are compared between the 2 clusters (*Right*). For example, a delta percent of +0.25 indicates that 25% more cells of choroidal endothelial cells express the gene above background than retinal endothelial cells.

Cluster Classification of CD31-Enriched Cell Populations in a Second Set of Donors. Of the 4,335 identified cells in our single-cell RNA-sequencing experiment, only 4% of the cells were classified as endothelial cells (*SI Appendix*, Table S1). Morphometric experiments suggest ∼15% of cells within the choroid are endothelial cells, indicating that endothelial cells may be underrepresented in the recovered single-cell population. Since choroidal endothelial cells provide the majority of oxygenated blood to the outer retina and degenerate early in AMD pathogenesis, we set out to more comprehensively characterize gene expression signatures of these cells. Eight RPE/choroid samples isolated from the macula and the periphery from 4 additional human donors were acquired before CD31 enrichment prior to single-cell RNA sequencing. Donors 5 to 7 had no documented ophthalmic history, while donor 4 was clinically diagnosed with neovascular AMD (Table 1).

A total of 14,234 cells were recovered after filtering, of which 7,647 were recovered from the macula and 6,587 were recovered from the periphery. UMAP dimensionality reduction was used to visualize the 13 identified clusters (Fig. 4*A*), and expression signatures of all clusters were compiled (Dataset S6). The expression of endothelial-specific genes and genes reported to be specific for different portions of the vascular tree were compared to the 13 identified clusters (Fig. 4*B*). Clusters 5 to 8 demonstrated strong and specific expression of *VWF* and were classified as endothelial cells (Fig. 4*C*). These endothelial clusters collectively contained 8,521 cells and constituted 60% of the recovered cells from this experiment (*SI Appendix*, Table S3), representing a 14.5-fold relative enrichment of endothelial cells compared to the initial single-cell RNA-sequencing study.

Clusters 5 and 6 were interpreted as endothelial cells derived from venules and/or veins, with high expression of the chemokine receptor *DARC* (35) and adhesion protein *MMRN1* (36), both of which have been reported to be vein specific. Cluster 7 consists of 1,013 cells classified as choriocapillaris endothelial cells, with high expression of membrane-associated carbonic anhydrase *CA4* (11) and *PLVAP*, which localizes to endothelial fenestrae (37). Cluster 8 consists of endothelial cells of arterial origin, with high expression of artery-enriched genes *FBLN2* and *SEMA3G* (36).

Differential expression analysis was performed to identify unique gene expression signatures of venous (clusters 5 and 6)-, choriocapillaris (cluster 7)-, and arterial (cluster 8)-derived endothelial cells (Fig. 4 *D–F* and Dataset S7). Arterial-derived cells demonstrate strong expression of gap-junction proteins GJA4 and GJA5 as well as Notch signaling protein HEY1, all of which regulate arteriogenesis (38, 39). In contrast, veins highly express many genes associated with leukocyte recruitment, including *DARC*, *SELE*, *VCAM1*, and *CCL23*. Endothelial cells originating from the choriocapillaris have more similar gene expression to veins than arteries (Fig. 4*G*). In addition to canonical choriocapillaris genes *CA4* and *PLVAP*, the choriocapillaris demonstrates specific expression of genes important in regulating barrier function (*SIPR3*, *SPARC*) (40, 41) and cellular adhesion (*PCDH12*) (42).

Arterial, venous, and capillary choroidal endothelial cells demonstrated strong gene expression differences between the different cell types. In contrast, gene expression differences between cells of macular versus peripheral origin in each cluster yielded more subtle differences (*SI Appendix*, Table S11). Although numerous statistically significant expression differences were identified between the macula and periphery, the log fold changes were modest.

The regulator of cell cycle gene (*RGCC*) was among the top 10 most enriched genes in the choriocapillaris (Dataset S8). Interestingly, *RGCC* has been observed to induce apoptosis in endothelial cells in response to complement MAC components C5b-9 (43). *RGCC* was the most up-regulated gene in the choriocapillaris of the donor with a diagnosis of advanced AMD compared to the 3 donors with normal ocular history (logFC = 1.27, 3.6× fold change)

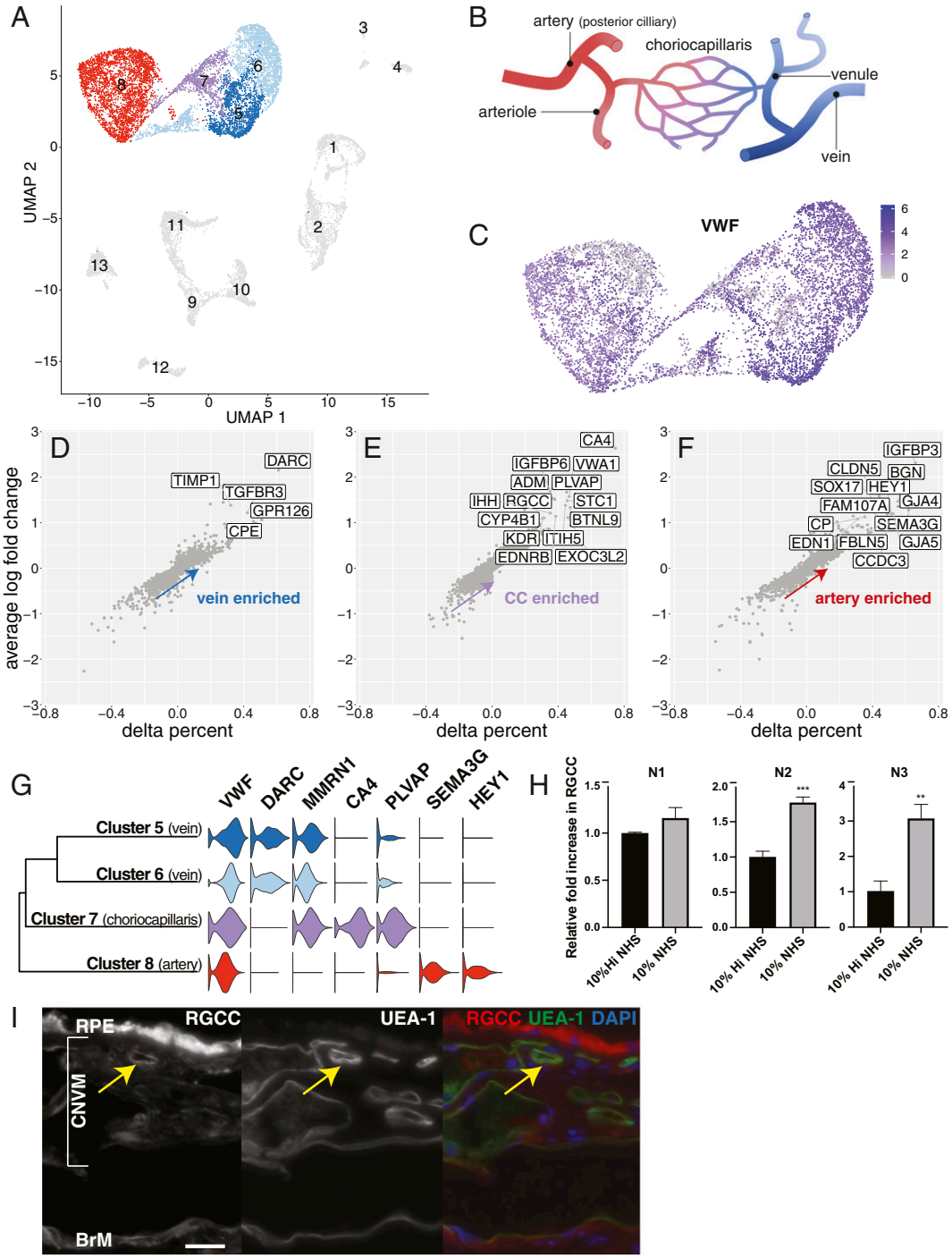

Fig. 4. Identification of choroidal vascular cell populations. (*A*) A second single-cell RNA-sequencing study was performed on 4 additional human donors. Endothelial cells were enriched prior to sequencing. A total of 14,234 cells were recovered after filtering, of which 8,521 (clusters 5 to 8) were classified as endothelial cells. (*B*) Choroidal vasculature consists of large caliber arteries and veins and an intermediary superficial capillary system known as the choriocapillaris. (*C*) The vast majority of cells in clusters 5 to 8 express the endothelial-specific transcript *VWF*. (*D–F*) Differential expression was performed to identify genes enriched in arterial (*D*), choriocapillaris (*E*), and vein (*F*) clusters. For each gene, the average log fold change and the percentage of cells that express the gene above background are compared between the 2 clusters (*Right*). For example, a delta percent of +0.25 indicates that 25% more cells of arterial endothelial cells express the gene above background than vein and choriocapillaris endothelial cells. (*G*) Hierarchical clustering of the top 100 most highly expressed genes in each cluster reveals that the choriocapillaris cluster has a more similar expression pattern to veins opposed to arteries. Expression of known endothelial (*VWF*), vein (*DARC*, *MMRN1*), choriocapillaris (*CA4*, *PLVAP*), and arterial (*HEY1*, *SEMA3G*) genes are compared across each endothelial cluster. (*H*) Expression of *RGCC*, 1 of the top 10 most enriched genes in the choriocapillaris cluster, was assessed by qPCR in an immortalized human choroidal endothelial cell line after treatment with 10% normal human serum (NHS, black) and 10% heat-inactivated serum (Hi NHS, gray) in 3 experiments (N1, N2, and N3). *RGCC* expression is increased in response to NHS compared to Hi NHS. $^{**}P < 0.01$ and $^{***}P < 0.001$. (*I*) Immunohistochemical localization of RGCC. A section through the macula of an 87-y-old donor with type I neovascular AMD was colabeled with RGCC, the endothelial-specific fucose binding lectin *Ulex europaeus* agglutinin-I (UEA-I), and DAPI. RGCC localizes to an endothelial cell (yellow arrow) within a choroidal neovascular membrane (CNVM). BrM, Bruch's membrane. Red fluorescence in the RPE is due to lipofuscin (an autofluorescent pigment); *RGCC* expression was not detected in the RPE cluster. (Scale bar: 25 μm.)

(Dataset S9). As *RGCC* has been previously shown to respond to complement activation, we treated an immortalized human choroidal cell line with 10% normal human serum (NHS), which contains all of the complement components required for complement activation and MAC (C5b-9) formation. The use of 10% heat-inactivated serum (HI NHS) served as a control, as complement in this serum is disabled. After 2 h of incubation, *RGCC* expression was assessed by RT-qPCR in 3 independent experiments (Fig. 4*H*) (*SI Appendix, Supplemental Methods*). *RGCC* expression was up-regulated in response to treatment with NHS compared to HI NHS in each experiment. In addition, we visualized RGCC localization with immunohistochemistry in a group of 5 independent donors with neovascular AMD (*SI Appendix, Supplemental Methods*). A representative image is shown (Fig. 4*I*), in which RGCC was observed in an endothelial cell within a choroidal neovascular membrane from an 87-y-old donor.

Discussion

Single-cell RNA sequencing has emerged as a powerful tool to study gene expression in heterogenous tissues such as the choroid. As opposed to bulk RNA sequencing, where transcripts from different cell types are aggregated and analyzed together, single-cell RNA sequencing allows for precise mapping of gene expression patterns to individual cell types (44). Several studies have characterized gene expression patterns in the retina at the single-cell level (32, 45–48), and a recent study has characterized single-cell expression patterns of human fetal retina and RPE (49). However, the single-cell transcriptome, to our knowledge, has not been described within the human choroid, a complex tissue vital for retinal function.

In the current study, we perform 2 single-cell RNA-sequencing experiments on paired macular and peripheral RPE/choroid tissue samples from 7 human donor eyes. In the first experiment, we generated a catalog of cell type-specific transcripts for all major cell populations within the choroid, including Schwann cells, melanocytes, endothelial cells, pericytes, fibroblasts, and leukocytes, as well as RPE cells. This dataset allows for precise mapping of multidimensional gene expression signatures to diverse human choroidal and RPE cell populations.

In addition to the expected cell classes, we identified 2 populations of Schwann cells. Differential expression analysis suggested that the populations correspond to myelinating and nonmyelinating Schwann cell phenotypes (*SI Appendix*, Fig. S2). The human choroid is innervated by cranial and sympathetic nerve processes (50) as well as resident ganglion cells (51). Interestingly, 64% of the nonmyelinating Schwann cells originated from the macula of the donor with neovascular AMD, and these Schwann cells demonstrated significantly increased expression of complement factor D (*CFD*) (*SI Appendix*, Fig. S2*G*). Further studies will be required to determine whether this increase in nonmyelinating Schwann cell frequency is in response to AMD-mediated damage or an independent donor-specific finding.

Previous studies have compared regional gene expression within the RPE and choroid at the bulk RNA level (19–23). We replicated several region-specific expression findings from bulk studies, such as decreased macular RPE *BEST1* expression (52) and increased macular RPE *WTBC1* expression (29). However, bulk RNA expression comparisons can be complicated by regional differences in cellularity. For example, in our previous bulk RNA-sequencing assessment of macular versus peripheral gene expression within the RPE and choroid, almost all RPE-specific genes were found to be enriched in the periphery. This finding is presumably due to an increased relative proportion of RPE cells in the peripheral punches. In the current investigation, the single-cell level of resolution allows for the characterization of regionally specific expression patterns that are not susceptible to differences in population density.

While 174 endothelial cells were recovered in our first single-cell RNA-sequencing experiment, all of these cells were grouped in the same cluster and we were unable to detect a distinct population of choriocapillaris endothelial cells. Vascular endothelial cells of the choriocapillaris are known to exhibit distinctive characteristics at the biochemical and structural levels. They express high levels of *ICAM1* at resting states (although this constitutive *ICAM1* expression increases during inflammatory challenge) (53–55), *PLVAP* (37) (a constituent of their fenestrae diaphragms), MHC class I antigens (56), and carbonic anhydrase IV (*CA4*) (11) in contrast to other ocular endothelial cells. These unique molecular features may contribute to the susceptibility of the choriocapillaris to molecular insults that are implicated in AMD pathogenesis. Most notably, the MAC accumulates at increasing levels within the extracellular matrix surrounding aging choriocapillaris in contrast to vascular beds in other tissues (57). In addition, aging choriocapillaris demonstrates loss of surface CD34 expression, which may lead to increased leukocyte extravasation (58). As choriocapillaris endothelial cell physiology is unique and damage to the choriocapillaris is strongly implicated in AMD, we performed a second single-cell RNA-sequencing experiment in an attempt to more precisely characterize its gene expression signature.

In our second single-cell RNA-sequencing experiment, we successfully recovered 8,521 endothelial cells, with 1,013 cells classified as choriocapillaris endothelial cells. Unsurprisingly, the 2 most differentially expressed genes specific for this cluster were choriocapillaris-specific *CA4* and *PLVAP*. In addition to these previously identified genes, this cluster of cells allowed us to identify numerous novel choriocapillaris-enriched genes (Dataset S7). For example, *S1PR3* expression, which has been implicated in VEGF and MMP-2 production (59), was highly specific within the choriocapillaris. Similar expression characterizations within arterial and venous endothelial cells were compiled and represent a report of the transcriptome along the choroidal vascular tree (Dataset S7).

One gene of particular interest in this study was *RGCC*, the sixth-most enriched gene in choriocapillaris endothelial cells. The *RGCC* gene product regulates the cell cycle and is activated in response to MAC formation (60). In endothelial cells, *RGCC* overexpression has been shown to slow cell growth and induce apoptosis (43). Interestingly, *RGCC* was the most enriched gene in the choriocapillaris from the donor with neovascular AMD compared to 3 non-AMD donors (logFC = 1.27). Within this donor with neovascular AMD, macular *RGCC* expression was over 50% higher than peripheral *RGCC* expression. As genetic variants resulting in increased complement deposition are among the highest risk factors for developing AMD, and maculas with AMD show significantly elevated levels of MAC compared to age-matched controls (reviewed in ref. 61), *RGCC* represents a compelling target that may contribute to complement-mediated choriocapillaris damage. Moreover, we demonstrate that *RGCC* expression is up-regulated in response to complement treatment in choroidal endothelial cells. Likewise, previous studies of RF/6A cells in vitro demonstrate increased expression of the *RGCC* rhesus macaque homolog *C13ORF15* in response to complement treatment (log2FC = 1.41, P = 0.03) (62). Last, we show that RGCC is localized to an endothelial cell within a macular choroidal neovascular membrane from a donor with neovascular AMD with immunohistochemistry. Functional studies are needed to further assess whether increased *RGCC* expression induces damage within the unique environment of the choroidal endothelium.

There are several limitations to the current investigation. First, the frequency of cell types recovered for single-cell sequencing is likely not fully reflective of the cellularity of the choroid. In our initial single-cell experiment, only 4% of our recovered cells were endothelial cells, while we find ∼15% of choroidal cell nuclei belong to cells labeled with CD34 by immunohistochemistry. This underrepresentation of endothelial cells may be reflective of our dissociation protocols readily releasing cell populations loosely

residing in connective tissue, such as resident or circulating leukocytes, while not liberating other cells more strongly embedded in the matrix. Likewise, while choriocapillaris endothelial cells are more abundant than their larger caliber endothelial cell counterparts, far fewer cells were recovered from the choriocapillaris in our CD31-enriched single-cell RNA-sequencing experiment, likely due to the encasing of choriocapillaris endothelial cells in the intercapillary pillars of Bruch's membrane. Second, while the use of 12-mm RPE/choroid punches allowed for the recovery of a sufficient number of enriched endothelial cells for single-cell RNA sequencing in the second experiment, the use of larger punches may limit the detection of regionally expressed genes, such as those in the subfoveal choriocapillaris. Third, while our inclusion of at least one donor in each single-cell RNA-sequencing experiment with a diagnosis of AMD allows for hypothesis generation, expression studies from additional donors with AMD will be necessary in order to generalize these findings to a larger population.

This study provides a rich resource for the community to investigate gene expression within the RPE and choroid, especially with respect to choroidal endothelial cell gene expression. As such, we have deposited our raw and processed data in GEO (GSE135922), and included supplemental tables detailing the average expression of all genes in each described cluster (Datasets S1 and S6). Taken together, these results enhance our understanding of normal choroidal physiology and shed light on gene expression patterns in affected versus spared cell populations in AMD. Such identification of the choroidal endothelial transcriptome is particularly relevant to understanding the role of choroidal vascular damage in macular degeneration.

Methods

Human Donor Eyes. Seven human donor eyes were used in this study (Table 1). Donations were acquired through the Iowa Lions Eye Bank with complete consent by donors' next of kin and in accordance with the Declaration of Helsinki. All tissue utilized for this study was acquired in the laboratory within 8 h of death and processed immediately. Human donor tissue was utilized in 2 distinct single-cell RNA expression experiments, as described below. An experimental overview is provided in *SI Appendix*, Fig. S3.

Single-Cell RNA-Sequencing Experiment 1: Unenriched RPE and Choroid.

Sample information. Three human donors (donors 1 to 3) were included in the first single-cell RNA-sequencing study of the RPE and choroid (Table 1). For each donor, 8-mm punches were obtained from the macula and the inferotemporal periphery (~9 mm inferotemporal to the foveal center). The combined RPE/choroid layer was dissected from the neural retina and the sclera, and the RPE/choroid underwent gentle dissociation into single-cell suspensions as described below.

Dissociation. RPE/choroid was dissected from neural retina and underlying sclera before incubation in 20 units/mL papain with 0.005% DNase (Worthington Biochemical Corporation). RPE/choroid and papain were incubated at 37 °C on a shaker and gently mechanically dissociated with a pipette every 15 min for 1.25 h. Dissociated cells were subsequently resuspended in albumin-ovomucoid inhibitor to quench papain activity.

Cryopreservation. Dissociated cells were immediately resuspended in DMSO-based Recovery Cell Cryopreservation Media (Life Technologies) and placed in a CryoSafe cooler (CryoSafe) to cool at 1 °C/min in a −80 °C freezer. After 3 to 8 h, frozen cells were subsequently placed in liquid nitrogen for storage.

Barcoding and library construction. Cryopreserved cells were rapidly thawed in a 37 °C water bath and resuspended to concentrations of 1,000 cells/μL in PBS with 0.04% nonacetylated BSA (New England Biolabs). Viability analysis was performed with the Annexin V/Dead Cell Apoptosis Kit (Life Technologies Corporation), and all samples had >90% live cells using the Countess II FL Automated Cell Counter (Thermo Fisher Scientific). Single cells were barcoded with the chromium system using the v3 single-cell reagent kit (10x Genomics). Barcoded libraries were pooled and sequenced on the HiSeq 4000 platform (Illumina) generating 150-base pair paired-end reads.

Computational analysis. FASTQ files were generated from basecall files with the bcl2fastq software (Illumina) by the University of Iowa Institute of Human Genetics. FASTQ files were subsequently mapped to the prebuilt hg19 genome with CellRanger (version 3.0.1) (63). Libraries from each experiment were aggregated to the same effective sequencing depth. Cells with unique gene counts fewer than 300 were eliminated, and cells with more than 6,000 unique genes per cell were removed to eliminate potential doublets. Log normalization of aggregated reads was performed with Seurat (version 3.0.2) using a scale factor of 10,000 (64).

Single-Cell RNA-Sequencing Experiment 2: Preenrichment for CD31$^+$ Endothelial Cells. In order to more closely examine the transcriptome of choroidal endothelial cells, we modified our dissociation protocol prior to a second single-cell sequencing experiment to shift the distribution of analyzed cells to include more endothelial cells. In this experiment, separate 12-mm punches of RPE/choroid were centered on the macula and on the periphery (~12 mm inferotemporal to the foveal center). Four human donors were included in this study (Table 1). Donors 5 to 7 had no documented ophthalmic history, while donor 4 had previously been diagnosed with neovascular AMD. After dissection away from the retina and sclera, the RPE/choroid was finely diced into small squares (~1 × 1 mm) with a razor blade. The resulting suspension was dissociated in 450 units/mL collagenase II (Gibco) reconstituted in Hank's balanced salt solution containing calcium chloride and magnesium chloride (Life Technologies) following a previously described protocol (65). RPE/choroid and collagenase II were incubated on a shaker at 37 °C for 1 h before cryopreservation, as described above.

Cryopreserved cells from donors 4 to 7 were rapidly thawed before preenrichment for endothelial cells. Cells were incubated for 15 min with anti-CD31 microbeads (Miltenyi Biotech) according to the manufacturer's instructions before automated autoMACs magnetic separation (Miltenyi Biotech) of the CD31$^+$ cell fraction. The positive cell fraction was passed 2 times through a 40-μm filter to remove aggregates. Single cells were immediately barcoded before library sequencing as described above. Cells with unique gene counts fewer than 500 were eliminated, and cells with more than 7,000 unique genes per cell were removed to eliminate potential doublets. Data were log-normalized before canonical correlation analysis aggregation was performed in Seurat.

Data Availability Statement. Raw and processed data have been deposited at GEO (https://www.ncbi.nlm.nih.gov/geo/) (accession no. GSE135922) (66).

ACKNOWLEDGMENTS. We thank the donors, their families, and the Iowa Lions Eye Bank for their generous role in this research. This work was supported in part by NIH Grants T32 GM007337, EY024605, EY027038, and P30 EY025580; the Elmer and Sylvia Sramek Charitable Foundation; Research to Prevent Blindness; and the Martin and Ruth Carver Chair in Ocular Cell Biology. The RGCC monoclonal antibody developed by Johns Hopkins University/CDI was obtained from the Developmental Studies Hybridoma Bank, created by the National Institute of Child Health and Human Development of the NIH and maintained at the Department of Biology, The University of Iowa (Iowa City, IA). The data presented herein were obtained at the Flow Cytometry Facility, which is a Carver College of Medicine/Holden Comprehensive Cancer Center Core Research Facility at the University of Iowa. The facility is funded through user fees and the generous financial support of the Carver College of Medicine, Holden Comprehensive Cancer Center, and Iowa City Veteran's Administration Medical Center.

1. T. M. Redmond *et al.*, Rpe65 is necessary for production of 11-*cis*-vitamin A in the retinal visual cycle. *Nat. Genet.* **20**, 344–351 (1998).
2. R. W. Young, D. Bok, Participation of the retinal pigment epithelium in the rod outer segment renewal process. *J. Cell Biol.* **42**, 392–403 (1969).
3. S. Y. Schmidt, R. D. Peisch, Melanin concentration in normal human retinal pigment epithelium. Regional variation and age-related reduction. *Invest. Ophthalmol. Vis. Sci.* **27**, 1063–1067 (1986).
4. J. Cai, K. C. Nelson, M. Wu, P. Sternberg, Jr, D. P. Jones, Oxidative damage and protection of the RPE. *Prog. Retin. Eye Res.* **19**, 205–221 (2000).
5. Y. Ban, L. J. Rizzolo, Regulation of glucose transporters during development of the retinal pigment epithelium. *Brain Res. Dev. Brain Res.* **121**, 89–95 (2000).
6. D. L. Nickla, J. Wallman, The multifunctional choroid. *Prog. Retin. Eye Res.* **29**, 144–168 (2010).
7. T. M. Nork *et al.*, Measurement of regional choroidal blood flow in rabbits and monkeys using fluorescent microspheres. *Arch. Ophthalmol.* **124**, 860–868 (2006).
8. T. Hasegawa *et al.*, The embryonic human choriocapillaris develops by hemo-vasculogenesis. *Dev. Dyn.* **236**, 2089–2100 (2007).
9. D. Abi-Hanna, D. Wakefield, S. Watkins, HLA antigens in ocular tissues. I. In vivo expression in human eyes. *Transplantation* **45**, 610–613 (1988).
10. R. F. Mullins, J. M. Skeie, E. A. Malone, M. H. Kuehn, Macular and peripheral distribution of ICAM-1 in the human choriocapillaris and retina. *Mol. Vis.* **12**, 224–235 (2006).
11. G. S. Hageman, X. L. Zhu, A. Waheed, W. S. Sly, Localization of carbonic anhydrase IV in a specific capillary bed of the human eye. *Proc. Natl. Acad. Sci. U.S.A.* **88**, 2716–2720 (1991).

12. K. L. Pennington, M. M. DeAngelis, Epidemiology of age-related macular degeneration (AMD): Associations with cardiovascular disease phenotypes and lipid factors. *Eye Vis. (Lond.)* **3**, 34 (2016).
13. J. Z. Nowak, Age-related macular degeneration (AMD): Pathogenesis and therapy. *Pharmacol. Rep.* **58**, 353–363 (2006).
14. S. Beatty, H. Koh, M. Phil, D. Henson, M. Boulton, The role of oxidative stress in the pathogenesis of age-related macular degeneration. *Surv. Ophthalmol.* **45**, 115–134 (2000).
15. K. R. Chirco, E. H. Sohn, E. M. Stone, B. A. Tucker, R. F. Mullins, Structural and molecular changes in the aging choroid: Implications for age-related macular degeneration. *Eye (Lond.)* **31**, 10–25 (2017).
16. R. F. Mullins, M. N. Johnson, E. A. Faidley, J. M. Skeie, J. Huang, Choriocapillaris vascular dropout related to density of drusen in human eyes with early age-related macular degeneration. *Invest. Ophthalmol. Vis. Sci.* **52**, 1606–1612 (2011).
17. A. Biesemeier, T. Taubitz, S. Julien, E. Yoeruek, U. Schraermeyer, Choriocapillaris breakdown precedes retinal degeneration in age-related macular degeneration. *Neurobiol. Aging* **35**, 2562–2573 (2014).
18. R. F. Mullins *et al*., The membrane attack complex in aging human choriocapillaris: Relationship to macular degeneration and choroidal thinning. *Am. J. Pathol.* **184**, 3142–3153 (2014).
19. S. S. Whitmore *et al*., Transcriptomic analysis across nasal, temporal, and macular regions of human neural retina and RPE/choroid by RNA-seq. *Exp. Eye Res.* **129**, 93–106 (2014).
20. L. Tian *et al*., Transcriptome of the human retina, retinal pigmented epithelium and choroid. *Genomics* **105**, 253–264 (2015).
21. H. Chen, B. Liu, T. J. Lukas, A. H. Neufeld, The aged retinal pigment epithelium/choroid: A potential substratum for the pathogenesis of age-related macular degeneration. *PLoS One* **3**, e2339 (2008).
22. A. M. Newman *et al*., Systems-level analysis of age-related macular degeneration reveals global biomarkers and phenotype-specific functional networks. *Genome Med.* **4**, 16 (2012).
23. S. S. Whitmore *et al*., Altered gene expression in dry age-related macular degeneration suggests early loss of choroidal endothelial cells. *Mol. Vis.* **19**, 2274–2297 (2013).
24. C. M. Stanton *et al*., Complement factor D in age-related macular degeneration. *Invest. Ophthalmol. Vis. Sci.* **52**, 8828–8834 (2011).
25. K. Yuan *et al*., Increased pyruvate dehydrogenase kinase 4 expression in lung pericytes is associated with reduced endothelial-pericyte interactions and small vessel loss in pulmonary arterial hypertension. *Am. J. Pathol.* **186**, 2500–2514 (2016).
26. C. S. Casey *et al*., Apolipoprotein E inhibits cerebrovascular pericyte mobility through a RhoA protein-mediated pathway. *J. Biol. Chem.* **290**, 14208–14217 (2015).
27. J. Lu, M. Chatterjee, H. Schmid, S. Beck, M. Gawaz, CXCL14 as an emerging immune and inflammatory modulator. *J. Inflamm. (Lond.)* **13**, 1 (2016).
28. Y. Hayashi *et al*., CXCL14 and MCP1 are potent trophic factors associated with cell migration and angiogenesis leading to higher regenerative potential of dental pulp side population cells. *Stem Cell Res. Ther.* **6**, 111 (2015).
29. S. S. van Soest *et al*., Comparison of human retinal pigment epithelium gene expression in macula and periphery highlights potential topographic differences in Bruch's membrane. *Mol. Vis.* **13**, 1608–1617 (2007).
30. M. Shibuya *et al*., Proteomic and transcriptomic analyses of retinal pigment epithelial cells exposed to REF-1/TFPI-2. *Invest. Ophthalmol. Vis. Sci.* **48**, 516–521 (2007).
31. D. V. Nguyen *et al*., An ocular view of the IGF-IGFBP system. *Growth Horm. IGF Res.* **23**, 45–52 (2013).
32. A. P. Voigt *et al*., Molecular characterization of foveal versus peripheral human retina by single-cell RNA sequencing. *Exp. Eye Res.* **184**, 234–242 (2019).
33. P. P. Zheng *et al*., Glut1/SLC2A1 is crucial for the development of the blood-brain barrier in vivo. *Ann. Neurol.* **68**, 835–844 (2010).
34. T. T. Hochgrebe, D. Humphreys, M. R. Wilson, S. B. Easterbrook-Smith, A re-examination of the role of clusterin as a complement regulator. *Exp. Cell Res.* **249**, 13–21 (1999).
35. A. Thiriot *et al*., Differential DARC/ACKR1 expression distinguishes venular from non-venular endothelial cells in murine tissues. *BMC Biol.* **15**, 45 (2017).
36. M. F. Sabbagh *et al*., Transcriptional and epigenomic landscapes of CNS and non-CNS vascular endothelial cells. *eLife* **7**, e36187 (2018).
37. L. Herrnberger, K. Ebner, B. Junglas, E. R. Tamm, The role of plasmalemma vesicle-associated protein (PLVAP) in endothelial cells of Schlemm's canal and ocular capillaries. *Exp. Eye Res.* **105**, 27–33 (2012).
38. J. S. Fang *et al*., Shear-induced Notch-Cx37-p27 axis arrests endothelial cell cycle to enable arterial specification. *Nat. Commun.* **8**, 2149 (2017).
39. I. Buschmann *et al*., Pulsatile shear and Gja5 modulate arterial identity and remodeling events during flow-driven arteriogenesis. *Development* **137**, 2187–2196 (2010).
40. B. A. Wilkerson, K. M. Argraves, The role of sphingosine-1-phosphate in endothelial barrier function. *Biochim. Biophys. Acta* **1841**, 1403–1412 (2014).
41. S. E. Goldblum, X. Ding, S. E. Funk, E. H. Sage, SPARC (secreted protein acidic and rich in cysteine) regulates endothelial cell shape and barrier function. *Proc. Natl. Acad. Sci. U.S.A.* **91**, 3448–3452 (1994).
42. A. Aran *et al*., Loss of function of PCDH12 underlies recessive microcephaly mimicking intrauterine infection. *Neurology* **86**, 2016–2024 (2016).
43. X. An *et al*., Response gene to complement 32, a novel hypoxia-regulated angiogenic inhibitor. *Circulation* **120**, 617–627 (2009).
44. B. Hwang, J. H. Lee, D. Bang, Single-cell RNA sequencing technologies and bioinformatics pipelines. *Exp. Mol. Med.* **50**, 96 (2018).
45. E. Z. Macosko *et al*., Highly parallel genome-wide expression profiling of individual cells using nanoliter droplets. *Cell* **161**, 1202–1214 (2015).
46. Y. R. Peng *et al*., Molecular classification and comparative taxonomics of foveal and peripheral cells in primate retina. *Cell* **176**, 1222–1237.e22 (2019).
47. B. A. Rheaume *et al*., Single cell transcriptome profiling of retinal ganglion cells identifies cellular subtypes. *Nat. Commun.* **9**, 2759 (2018).
48. K. Shekhar *et al*., Comprehensive classification of retinal bipolar neurons by single-cell transcriptomics. *Cell* **166**, 1308–1323.e30 (2016).
49. Y. Hu *et al*., Dissecting the transcriptome landscape of the human fetal neural retina and retinal pigment epithelium by single-cell RNA-seq analysis. *PLoS Biol.* **17**, e3000365 (2019).
50. A. Reiner, M. E. C. Fitzgerald, N. Del Mar, C. Li, Neural control of choroidal blood flow. *Prog. Retin. Eye Res.* **64**, 96–130 (2018).
51. C. Flügel, E. R. Tamm, B. Mayer, E. Lütjen-Drecoll, Species differences in choroidal vasodilative innervation: Evidence for specific intrinsic nitrergic and VIP-positive neurons in the human eye. *Invest. Ophthalmol. Vis. Sci.* **35**, 592–599 (1994).
52. R. F. Mullins, M. H. Kuehn, E. A. Faidley, N. A. Syed, E. M. Stone, Differential macular and peripheral expression of bestrophin in human eyes and its implication for best disease. *Invest. Ophthalmol. Vis. Sci.* **48**, 3372–3380 (2007).
53. D. S. McLeod, D. J. Lefer, C. Merges, G. A. Lutty, Enhanced expression of intracellular adhesion molecule-1 and P-selectin in the diabetic human retina and choroid. *Am. J. Pathol.* **147**, 642–653 (1995).
54. J. M. Skeie, J. H. Fingert, S. R. Russell, E. M. Stone, R. F. Mullins, Complement component C5a activates ICAM-1 expression on human choroidal endothelial cells. *Invest. Ophthalmol. Vis. Sci.* **51**, 5336–5342 (2010).
55. S. Zeng, J. Hernández, R. F. Mullins, Effects of antioxidant components of AREDS vitamins and zinc ions on endothelial cell activation: Implications for macular degeneration. *Invest. Ophthalmol. Vis. Sci.* **53**, 1041–1047 (2012).
56. S. V. Goverdhan *et al*., Association of HLA class I and class II polymorphisms with age-related macular degeneration. *Invest. Ophthalmol. Vis. Sci.* **46**, 1726–1734 (2005).
57. K. R. Chirco, B. A. Tucker, E. M. Stone, R. F. Mullins, Selective accumulation of the complement membrane attack complex in aging choriocapillaris. *Exp. Eye Res.* **146**, 393–397 (2016).
58. E. H. Sohn *et al*., Loss of CD34 expression in aging human choriocapillaris endothelial cells. *PLoS One* **9**, e86538 (2014).
59. H. Y. Sun, S. P. Wei, R. C. Xu, P. X. Xu, W. C. Zhang, Sphingosine-1-phosphate induces human endothelial VEGF and MMP-2 production via transcription factor ZNF580: Novel insights into angiogenesis. *Biochem. Biophys. Res. Commun.* **395**, 361–366 (2010).
60. T. Badea *et al*., RGC-32 increases p34CDC2 kinase activity and entry of aortic smooth muscle cells into S-phase. *J. Biol. Chem.* **277**, 502–508 (2002).
61. K. R. Chirco *et al*., Evaluation of serum and ocular levels of membrane attack complex and C-reactive protein in CFH-genotyped human donors. *Eye (Lond.)* **32**, 1740–1742 (2018).
62. S. Zeng *et al*., Molecular response of chorioretinal endothelial cells to complement injury: Implications for macular degeneration. *J. Pathol.* **238**, 446–456 (2016).
63. G. X. Y. Zheng *et al*., Massively parallel digital transcriptional profiling of single cells. *Nat. Commun.* **8**, 14049 (2017).
64. A. Butler, P. Hoffman, P. Smibert, E. Papalexi, R. Satija, Integrating single-cell transcriptomic data across different conditions, technologies, and species. *Nat. Biotechnol.* **36**, 411–420 (2018).
65. J. C. Giacalone *et al*., Generation of an immortalized human choroid endothelial cell line (iChEC-1) using an endothelial cell specific promoter. *Microvasc. Res.* **123**, 50–57 (2019).
66. A. P. Voigt *et al*., Single-cell transcriptomics of the human retinal pigment epithelium and choroid in health and macular degeneration. Gene Expression Omnibus. https://www.ncbi.nlm.nih.gov/geo/query/acc.cgi?acc=GSE135922. Deposited 17 August 2019.